

# Design of thin wall structures for energy absorption applications: Enhancement of crashworthiness due to axial and oblique impact forces



F. Tarlochan<sup>a,\*</sup>, F. Samer<sup>b</sup>, A.M.S. Hamouda<sup>c</sup>, S. Ramesh<sup>d</sup>, Karam Khalid<sup>a</sup>

<sup>a</sup> Center for Innovation and Design, Universiti Tenaga Nasional, Kajang, Malaysia

<sup>b</sup> College of Engineering, University of Anbar, Anbar, Iraq

<sup>c</sup> Department of Mechanical and Industrial Engineering, Qatar University, Doha, Qatar

<sup>d</sup> Centre of Advanced Manufacturing & Materials Processing (AMMP), Department of Engineering Design and Manufacture, Faculty of Engineering, University of Malaya, Kuala Lumpur, Malaysia

## ARTICLE INFO

### Article history:

Received 3 January 2013

Accepted 9 April 2013

Available online 6 June 2013

### Keywords:

Crashworthiness  
Energy absorption  
Oblique impact  
Axial impact

## ABSTRACT

This paper describes a computationally aided design process of a thin wall structure subject to dynamic compression in both axial and oblique directions. Several different cross sectional shapes of thin walled structures subjected to direct and oblique loads were compared initially to obtain the cross section that fulfills the performance criteria. The selection was based on multi-criteria decision making (MCDM) process. The performance parameters used are the absorbed crash energy, crush force efficiency, ease of manufacture and cost. Once the cross section was selected, the design was further enhanced for better crash performances by investigating the effect of foam filling, increasing the wall thickness and by introducing a trigger mechanism. The outcome of the design process was very encouraging as the new design was able to improve the crash performance by an average of 10%.

© 2013 Elsevier Ltd. All rights reserved.

## 1. Introduction

Today's society is placing increased dependence on transportation systems. This can be seen clearly by the continuously increasing number of vehicles over the last two decades. With the increase in vehicles, the number of collisions and fatalities has also increased [1]. In view of this, higher demand has been advocated to ensure higher standards of safety in vehicles. This has led to continuous research in designing efficient energy absorbers to dissipate energy during an accident whilst protecting the occupant in the vehicle. Thin wall structures or tubes have been extensively used as these energy absorbers most commonly exist as either square or circular cross sections [1–5]. These structures are called the frontal longitudinal and are shown in Fig. 1. Such structures permanently deform to mitigate the crash energy and forces transmitted to the vehicle reducing the decelerations experienced by the occupants.

Extensive research has been carried out in improving the energy absorption of such structures due to direct axial impact [6]. However in the context of a vehicle collision, the vehicles energy absorbers are commonly subjected to both axial and

oblique (off-axis) loads. In comparison with axial loading conditions, relatively few studies have been conducted on the energy absorption response of thin walled tubes under oblique loads [7]. Some of the well cited works in this oblique impact are works of Borvik et al. [8], Reyes et al. [9–11] and Reid et al. [12]. Constraints imposed on the layout of the engine components and their mounting requirements have however led to the inefficient geometric and stiffness designs of the frontal longitudinal tubes. The inefficiency in design causes the frontal longitudinal tubes to collapse in a bending mode rather than progressive axial crushing [13]. These imperfections cause the frontal longitudinal tubes to collapse in a bending mode rather than progressive axial crushing [13], especially when the impact is not exactly frontal but offset and oblique. This leads to a lower energy absorption capability of the frontal longitudinal structure.

In addition to this, other researchers have also considered foams as a design variable whilst designing for energy absorption. Foams, be it metal or polymer based, have been studied extensively as fillers for tubular structures [10,14–20]. The findings show that the usage of foam tends to increase the energy absorption capability of such tubular structures while decreasing the energy absorption stroke (crush length of tube). This is useful in designing compact cars.

Recently, there is a trend amongst researchers in terms of shifting from experimental to computer simulation (finite element

\* Corresponding author. Tel.: +60 3 89212224; fax: +60389212116.  
E-mail address: [faristarlochan@gmail.com](mailto:faristarlochan@gmail.com) (F. Tarlochan).

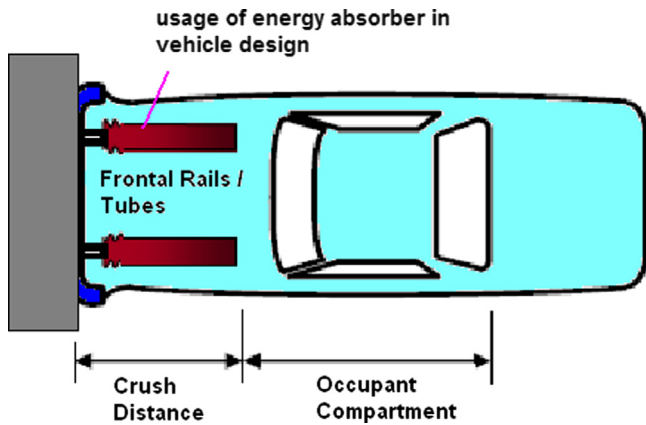


Fig. 1. Frontal longitudinal thin wall structure [3].

analysis—FEA) based studies. FEA is a technique widely used globally in design, analysis and optimization. For impact studies, FEA is shown to be a useful tool to understand the deformation mechanism and responses of energy absorber tubes under impact loads [6,21,22]. The FEA simulations reduce the need to manufacture expensive prototypes for physical testing and aid in comparison and improvement of different concepts. Hence, the objective of this study is the design of an efficient thin wall tube energy absorber with foam packing subjected to both axial and oblique loading. The study is carried out using a finite element analysis.

## 2. Design methodology and performance indicators

This study was broken up into three phases. In the first phase, six different thin walled tubular cross sectional profiles were designed. These cross sectional profiles include circular, square, rectangle, hexagonal, octagonal and ellipse profiles. The tubular structural material was modeled as A36 steel (mild steel). While designing these structures, the perimeter of the cross section, the length and the thickness of the tubes were made constant for all the seven tubular profiles. This was done to solely investigate various cross sectional profile crash performances. The length and thickness were chosen to be 350 mm and 2 mm respectively. For the cross sectional perimeter, 2 sets were chosen, namely 372 mm and 300 mm for all tube profiles. These values were chosen based on the average perimeter calculated from most sedan and compact cars found in the local market. From these six profiles, one profile was chosen after undergoing a multi-criteria decision making (MCDM) process. The second phase of the study was to further enhance the crash performance of the chosen profile from the first phase of the study. Here the crash performance was enhanced by including a filler material into the tube, namely aluminum foam with a density of 534 kg/m<sup>3</sup>. The dynamic simulations for both phases include direct and oblique loading of 30° off the tubular longitudinal axis. This value of 30° was chosen because it was found that the highest load enhancement without major reduction in mean force happens at 30° [33,3]. The initial impact velocity was set to be 15.6 m/s with an impacting mass of 275 kg. These values are discussed in detail in the following section. The final phase was the enhancement of the crash performance by the addition of a trigger mechanism. The trigger mechanism helps to initiate progressive collapse of structures. Details of the design of experiment are given in Table 1.

In terms of the performance indicators, two broad categories were considered. The main performance indicator is to evaluate the overall crash response and the secondary is to evaluate the issues on the cost and the feasibility (ease of manufacturing and

assembly). Under the crash response, the following parameters were obtained (with reference to Fig. 2):

- Peak force,  $F_{MAX}$   
The peak force of a component is the highest load required to cause significant permanent deformation or distortion. The peak load is of concern for two reasons. The first is that at low-speed and low-energy impacts, it is desirable that no permanent deformation takes place, as this would be considered as a damage to the structure. Secondly the peak load is often the maximum load observed in the useful stroke of the energy absorbing device and as such has a direct importance on the loading of the vehicle occupant. In the simulation, the peak load is measured off from the reaction force at the fixed base, a similar principle on how load cells are used in actual physical tests.

- Energy absorption,  $E_s$   
In Fig. 2 the total energy absorbed,  $U$ , in crushing the structure is equal to the area under the load–displacement curve, where,

$$U = \int_0^{d_{max}} F dS \quad (1)$$

The specific energy absorption is defined as the energy absorbed per unit mass of material as given in the following equation.

$$E_s = \frac{U}{m}, \quad (2)$$

where  $m$  is the crushed mass of the component.

- Crush force efficiency,  $CFE$


The average and peak forces are important parameters to be determined as they are directly related to the deceleration that will be experienced by the vehicle occupants. The best way to quantify this is by defining a crush force efficiency parameter, which is the ratio of the mean force to the peak force. This ratio is defined as the crush force efficiency. If the ratio is close to unity, the absorber is crushing at a value close to the peak load, hence minimizing the changes in deceleration, as desired from any absorber design. On the other hand, if this ratio is away from unity, there are rapid changes in the deceleration and this is dangerous to have in the design of a vehicle. In general, as the CFE value approaches unity, the better is the performance of the energy absorbing structure [1].

The ideal energy absorber would attain a maximum load immediately and maintain it for the entire length of the component. In summary, the design goals for an efficient energy absorption device are to have a mean load equivalent to the peak load and to have a high specific energy absorption capability.

For the multi-criteria decision making (MCDM) process, the complex proportional assessment method (COPRAS) was chosen [23,24]. This method was chosen for its simplicity in usage. The method assumes direct and proportional dependences of the significance and utility degree of the available alternatives under the presence of mutually conflicting criteria. It takes into account the performance of the alternatives with respect to different criteria and the corresponding criteria weights [23]. This method selects the best decision considering both the ideal and the least preferred solution. The COPRAS method is a successful method to solve problems of design selection in many fields like construction, project management, and economy. This method consists of many steps, and they are explained as follows:

Step 1: *Developing the initial matrix (X) and finding the relative coefficient (R)*

**Table 1**  
Geometry and dimensions of tubes used for study.

Profile	Specimen ID	Perimeter (mm)	Length (mm)	Mass (kg)	Major Dimension (mm)	Thickness (mm)	Profile
Circular	C_300	300	350	1.7	Diam.=95.5	2	
	C_372	372		2.0	Diam.=118.1		
Rectangle	R_300	300	350	1.7	90 × 60	2	
	R_372	372		2.0	112 × 74		
Square	S_300	300	350	1.7	75 × 75	2	
	S_372	372		2.0	93 × 93		
Hexagonal	H_300	300	350	1.7	50 each side	2	
	H_372	372		2.0	62		
Octagonal	O_300	300	350	1.7	37.5 each side	2	
	O_372	372		2.0	46.5		
Ellipse	E_300	300	350	1.7	62,31	2	
	E_372	372		2.0	74,37		

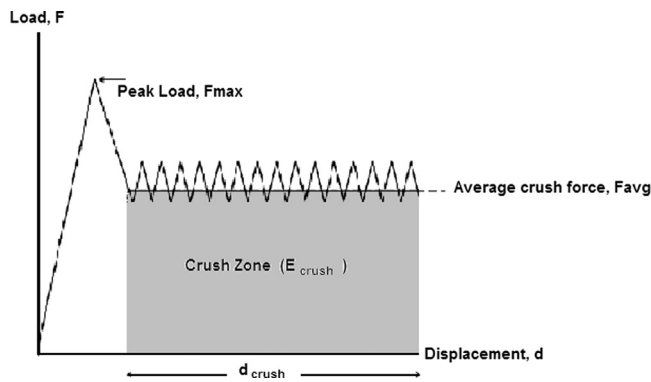


Fig. 2. Typical force–displacement diagram.

This first step involves generating a simple matrix which maps the alternatives (design concepts) to the selection criteria. This matrix is labeled as  $X$  as given in the following equation.

$$X = [x_{ij}]_{m \times n} = \begin{bmatrix} x_{11} & x_{12} & \dots & x_{1n} \\ x_{21} & x_{22} & \dots & x_{2n} \\ \vdots & \vdots & \vdots & \vdots \\ x_{m1} & x_{m2} & \dots & x_{mn} \end{bmatrix} \quad (i = 1, 2, \dots, m), (j = 1, 2, \dots, n) \quad (3)$$

where  $x_{ij}$  is the performance value of the  $i$ th alternative on the  $j$ th criterion,  $m$  is the number of alternatives (design concepts) compared and  $n$  is the number of criteria. The problem in design selection is that most design criteria are not in the same dimensions or units. This makes the selection a little harder. One way to overcome this is to convert the entire matrix  $X$  to a non-dimensionalized matrix  $R$ . This way, it is easier to compare between selection criteria. The entry  $x_{ij}$  represents the positive (absolute) value for each criteria and  $\sum x_{ij}$  is the summation for a number of positive decisions. The importance of the relative coefficient is to reduce the values of the criteria to make it easy for comparison. The symbol of the relative coefficient is  $R$  and it is

**Table 2**  
Example of weightage setting.

Selection criteria	Number of comparison sets, $N=5(5-1)/2=10$										$W_j$	$w_j$
	1	2	3	4	5	6	7	8	9	10		
A	3	3	2	2							10	10/40=0.25
B	1				2	1	2				6	6/40=0.15
C		1				2		2	1		6	6/40=0.15
D			2			3		2		2	9	9/40=0.225
E				2			2		3	2	9	9/40=0.225
	Total, $\Sigma$										<b>G=40</b>	<b>1</b>

formulated as

$$R = [r_{ij}]_{m \times n} = \frac{x_{ij}}{\sum_{i=1}^m x_{ij}} \quad (4)$$

Step 2: Determining the weighted normalized decision matrix  $D$ .

$$D = [y_{ij}] = r_{ij} \times w_j \quad (5)$$

where  $r_{ij}$  is the normalized performance value of the  $i$ th alternative on the  $j$ th criterion and  $w_j$  is the weight of the  $j$ th criterion. The summation of the normalized weight for each criterion is always equal to the weight of the same mentioned criterion as given in the following equation.

$$\sum_{i=1}^m y_{ij} = w_j \quad (6)$$

To determine or compute the individual weightage for each criteria  $w_j$ , the following method can be used:

- Compare two criteria at a time. Total comparison sets ( $N$ ) are equal to  $N = (n(n-1)/2)$  where  $n$  is the number of selection criteria.
- Amongst the two criteria being selected, the criterion which is more important is given a score of 3 whereas the criterion which is least important is given a score of 1. If both criteria are

of equal importance, a score of 2 is given. Repeat this for all other criteria.

- The total score obtained for each criteria is computed as  $\sum_{i=1}^m N_{ij} = W_j$ .
- A relative emphasis weighting factor,  $w_j$ , for each selection criteria is obtained by dividing the total score for each selection criteria ( $W_j$ ) by the global total score  $\sum_{j=1}^m W_j = G$  (refer Table 2 for example).

#### Step 3: Summing of beneficial and non-beneficial attributes

The values of the normalized decision matrix contain beneficial and non-beneficial attributes. A low value of a non-beneficial attribute is better for the selection. On the other hand, the greater is the value of a beneficial attribute, the better is the selection possibility. The next step is to separate them by their sums. These sums are formulated into two equations:

$$S_{+1} = \sum_{j=1}^n 1Y_{+ij} \quad (7)$$

$$S_{-1} = \sum_{j=1}^n 1Y_{-ij} \quad (8)$$

where  $y_{+ij}$  and  $y_{-ij}$  are the weighted normalized values for the beneficial and non-beneficial attributes respectively. The greater the value of  $S_{+i}$ , the better is the design concept, and the lower the value of  $S_{-i}$ , the better is the design concept. Just to note  $\sum S_{+i}$  and  $\sum S_{-i}$  of the design concepts are always respectively equal to the sums of weights for the beneficial and non-beneficial attributes as expressed by the following equations:

$$Sum_{positive} = \sum_{i=1}^m S_{+i} = \sum_{i=1}^m \sum_{j=1}^n 1Y_{+ij} \quad (9)$$

$$Sum_{negative} = \sum_{i=1}^m S_{-i} = \sum_{i=1}^m \sum_{j=1}^n 1Y_{-ij} \quad (10)$$

The summation of Eqs. (9) and (10) is always equal to one.

#### Step 4: Relative significance or priority (Q)

The priorities of the design concepts are calculated based on the notion of relative significance ( $Q_i$ ). The greater the value of  $Q_i$ , the higher is the priority of the design concept. The relative significance value of a design concept shows the degree of satisfaction attained by that concept. The design concept with the maximum relative significance  $Q_{max}$  is the best choice for the concept selection decision. The relative significance has been formulated as below:

$$Q_i = S_{+i} + \frac{S_{-min} \sum_{i=1}^m S_{-i}}{S_{-i} \sum_{i=1}^m (S_{-min}/S_{-i})} \quad (11)$$

where  $S_{-min}$  is the minimum value of  $S_{-i}$ .

#### Step 5: Determining the quantitative utility (U)

The value of the quantitative utility is related directly to the relative significance. The values with the quantitative utility complete the ranking of the alternatives and can be denoted as the formula below:

$$U_i = \frac{Q_i}{Q_{max}} \quad (12)$$

The maximum value of the relative significance is denoted as  $Q_{max}$ . The quantitative utility is directly proportional to the relative significance and the utility value with 100 is considered to be the best design using this method.

### 3. Finite element modeling

For a point in a body, time-dependent deformation for a point in a continuum can be found by using the following momentum equation:

$$\sigma_{ij} + \rho f_i = \rho \ddot{x}_i \quad (13)$$

where  $\sigma_{ij}$  is the Cauchy stress,  $\rho$  is the density,  $f_i$  is the body force and  $\ddot{x}_i$  is the acceleration.

Eq. (13) can be translated to the principle of virtual work by using the divergence theorem:

$$\int_V \rho \ddot{x}_i \delta x_i dV + \int_V \sigma_{ij} \delta x_{i,j} dV - \int_V \rho f_i \delta x_i dV - \int_{S^2} t_i \delta x_i dS = 0 \quad (14)$$

In terms of matrix form:

$$\sum_{i=1}^n \left\{ \int_V \rho N^t Nadv + \int_V B^t \sigma dv - \int_V \rho N^t b dv - \int_A N^t F dA + \int_S N^t F_c ds \right\}^i = 0 \quad (15)$$

where  $n$  is the number of elements,  $\sigma$  is the stress column vector,  $N$  is the interpolation matrix,  $a$  is the nodal acceleration column vector,  $B$  is the strain matrix,  $b$  is the body load column vector and finally  $F$  is the applied traction load (if any). This can also be explained in a more general term as given in the following equation.

$$[M] \left[ \frac{d^2 u}{dt^2} \right] + [C] \left[ \frac{du}{dt} \right] + [K] \{U\} = [F(t)] \quad (16)$$

where  $M$  is the mass matrix,  $C$  is the damping matrix and  $K$  is the stiffness matrix. Once the displacements are solved based on given initial loading and boundary conditions, plastic strains, contact forces and the energies such as internal and kinetic energies are computed. Most of the available finite element softwares commonly solve such a dynamic equilibrium equation in an implicit way, but for nonlinear dynamic problems such as crash, an explicit time integration scheme such as central difference method is preferred. In explicit method, the total time is divided into much smaller time intervals called time steps or increments. The dynamic equilibrium equations as given in Eq. (1) are solved and the values of the variables are determined at  $(t+\Delta t)$  based on the knowledge of their values at time  $t$ . In the explicit methods, data at time step  $n+1$  can be obtained from the previous time step ( $n$ ) and there is no dependence on the current time step. On the other hand, implicit methods are those where the information at time step  $n+1$  is dependent on the previous time steps and also on the current time step, making it difficult to solve.

In this study, finite element (FE) models of empty and foam filled tubes were developed using the non-linear FE code ABAQUS-Explicit. The code was used to predict the response of the thin wall tubes subjected to a free falling impinging mass. The entire model in this study comprises principally of the thin wall structure under study, the striker, and the base. The thin wall structure was modeled by using 4 node shell continuum (S4R) elements with 5 integration points along the thickness direction of the element. The foam was modeled using 8-noded continuum elements with the reduced integration techniques in combination with the hourglass control. Enhancement-based hourglass control was used to avoid artificial zero energy deformation modes and reduced integration was used to avoid volumetric locking. Element sizes of 5 mm were chosen for the shells and foam elements, based on a mesh convergence study. A mesh convergence is important to ensure a sufficient mesh density to accurately capture the deformation process. The contact algorithm used to simulate contact interaction between all components was the "general contact algorithm". This is important to avoid interpenetration of tube wall. This algorithm is less intense in terms of computational time. Contacts between the tube walls, with and without foam, were modeled as finite sliding penalty based contact algorithm with contact pairs and hard contact. The value of the Coulomb friction coefficient for all contact surfaces was set at 0.2 [24,25,27].

The striker was modeled as a rigid body with only one allowable translational displacement and all other translational and rotations



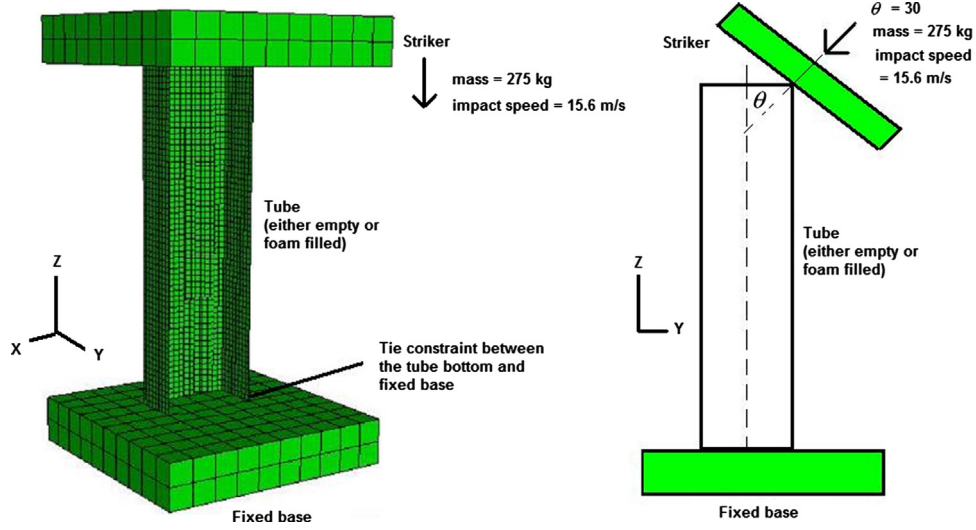


Fig. 3. Finite element analysis setup for direct and oblique impact.

Table 3  
Summary of parameters for A36 steel [26].

Parameter	Value	Description
A	146.7 MPa	Material parameter
B	896.9 MPa	Material parameter
N	0.320	Strain power coefficient
C	0.033	Material parameter
M	0.323	Temperature power coefficient
$\dot{\epsilon}_0$	1.0 s <sup>-1</sup>	Reference strain rate
$\rho$	7850 kg/m <sup>3</sup>	Density
T <sub>m</sub>	1773 K	Melting temperature
C <sub>p</sub>	486 J/kg·°K	Specific heat

degree of freedom were fixed. The impact velocity of the striker on the tubes was modeled to be 15.6 m/s (56 km/h) with a lumped mass of 275 kg (Fig. 3). The impact speed value was taken from the New Car Assessment Program (NCAP) by the National Highway Traffic Safety Administration (NHTSA). The mass was assumed to be 25% of a compact car (1100 kg). It was assumed that each tubular energy absorbing structure is capable of absorbing an equivalent kinetic energy of 275 kg mass since in reality the maximum energy that can be absorbed by two tubes in service is much less than 50% [25].

The tubular structure material in the FE model was modeled as A36 steel as it is the most commonly available one of the hot-rolled carbon steels. The material characterization of A36 was done as per Johnson–Cook constitutive isotropic hardening model. It is a phenomenological model that takes into account the strain hardening, strain rate effects and thermal softening. It is suitable for problems where the strain rate varies over a large range and the temperature changes due to plastic deformation caused by thermal softening [28]. These important material characteristics are combined in a multiplicative manner as given in Eq. (3) [29]:

$$\sigma_T = \left[ A + B(\dot{\epsilon}_{eff}^p)^N \right] \left( 1 + C \ln \frac{\dot{\epsilon}_{eff}^p}{\dot{\epsilon}_0} \right) \left[ 1 - \left( \frac{T - T_0}{T_{melt} - T_0} \right)^M \right] \quad (14)$$

where  $\sigma_T$  is the dynamic flow stress,  $\dot{\epsilon}_{eff}^p$  is the effective plastic strain,  $\dot{\epsilon}_{eff}^p$  is the effective plastic strain rate,  $\dot{\epsilon}_0$  is a reference strain rate, A, B, N, M and C are the material parameters and  $T_{melt}$  is the melting temperature whereas  $T_0$  is the transition temperature. The transition temperature is defined as the one at or below which there is no temperature dependence on the expression of the yield stress. It is usually taken as the room temperature of 293–297°K

Table 4  
Summary of parameters for aluminum foam model [31].

$\rho_f$ (kg/m <sup>3</sup> )	$\sigma_p$ (MPa)	$\alpha$	$\alpha_2$ (MPa)	$\beta$	$\gamma$	$\epsilon_D$
534	12.56	2.12	1544	3.680	1.00	1.6206

[28,30]. The summary of the Johnson–Cook parameters are given in Table 3 [30].

The plastic behavior of the aluminum foam is taken into account using the CRUSHABLE FOAM and the CRUSHABLE FOAM HARDENING options in the ABAQUS/Explicit software package which in turn is based upon the foam model of Dehspande and Fleck [31]. In this model, the following yield criterion is assumed:

$$F = \hat{\sigma} - Y \leq 0 \quad (15)$$

where

$$\hat{\sigma}^2 = \frac{1}{[1 + (\alpha/3)^2]} [\sigma_e^2 + \alpha \sigma_m^2] \quad (16)$$

The effective von Mises stress is defined as  $\sigma_e$  whereas the mean stress is defined as  $\sigma_m$ . Y in the equation denotes the yield strength [32]. The material parameter  $\alpha$  which defines the shape of the yield surface is a function of the plastic coefficient of contraction  $\nu_p$ . This coefficient is the plastic Poisson's ratio for aluminum foam, and is assumed to be zero [33,34] and is given as

$$\alpha^2 = \frac{2(1 - 2\nu_p)}{9(1 + \nu_p)} \quad (17)$$

To take into account strain hardening, the following equation is incorporated into the initial model in the software. The strain hardening effect is given by

$$Y = \sigma_p + \gamma \frac{\hat{\epsilon}}{\epsilon_D} + \alpha_2 \ln \left[ \frac{1}{1 - (\hat{\epsilon}/\epsilon_D)^\beta} \right] \quad (18)$$

The plateau stress  $\sigma_p$ , the parameters  $\alpha_2$ ,  $\gamma$ ,  $\epsilon_D$  and  $\beta$  are the material property constants, and  $\hat{\epsilon}$  is the effective strain. The densification strain  $\epsilon_D$  can be given as

$$\epsilon_D = -\frac{9 + \alpha^2}{3\alpha^2} \ln \left( \frac{\rho_f}{\rho_{f0}} \right) \quad (19)$$

**Table 5**  
Summary of crashworthiness parameters for all tube profiles for two different parameters (direct loading).

Indicators	Circular		Rectangle		Square		Hexagonal		Octagonal		Ellipse	
	C-Direct 300	C-Direct 372	R-Direct 300	R-Direct 372	S-Direct 300	S-Direct 372	H-Direct 300	H-Direct 372	O-Direct 300	O-Direct 372	E-Direct 300	E-Direct 372
Energy (kJ)	23.67	24.49	19.22	19.24	23.22	27.44	26.67	29.49	23.90	26.96	17.29	19.31
$P_{max}$ (kN)	207.84	242.09	205.36	206.12	208.92	260.44	213.55	255.90	207.65	250.50	187.16	236.11
CFE	0.55	0.49	0.46	0.46	0.55	0.52	0.60	0.59	0.55	0.52	0.46	0.39
$F_{average}$ (kN)	114.58	119.12	94.33	94.34	115.78	135.60	127.84	150.11	115.02	130.03	85.87	93.05

**Table 6**  
Summary of crashworthiness parameters for all tube profiles for two different parameters (oblique loading).

Indicators	Circular		Rectangle		Square		Hexagonal		Octagonal		Ellipse	
	C-Oblique 300	C-Oblique 372	R-Oblique 300	R-Oblique 372	S-Oblique 300	S-Oblique 372	H-Oblique 300	H-Oblique 372	O-Oblique 300	O-Oblique 372	E-Oblique 300	E-Oblique 372
Energy (kJ)	12.81	16.01	13.04	11.83	10.95	12.40	15.96	15.04	12.22	16.29	14.54	14.50
$P_{max}$ (kN)	153.82	174.11	134.04	106.30	148.23	197.17	132.53	116.75	142.51	178.01	130.18	177.93
CFE	0.41	0.46	0.48	0.56	0.36	0.31	0.59	0.64	0.42	0.46	0.56	0.40
$F_{average}$ (kN)	62.33	80.11	64.17	59.02	53.58	60.90	77.89	74.79	59.48	81.19	72.43	71.09

where  $\rho_f$  is the foam density and  $\rho_{fo}$  is the density of the base material [32,33]. Material parameters of foam filler used in the dynamic simulation are tabulated in Table 4 [33].

#### 4. Results and discussion

A summary of the results obtained in this study is presented in Tables 5 and 6 for convenience. Detailed discussions and explanations will be given in the accompanying sub-sections.

##### 4.1. Force–displacement characteristics of different geometric profiles

Typical force–displacement diagrams for each kind of profile tested in this study are presented in Figs. 4–9. The displacement here refers to the displacement of the rigid striker which is assumed to be in full contact with the tube as the tube crushes. Each figure depicts the force response for certain cross sectional geometric profile due to the direct and oblique loading for the two classes of perimeters (373 mm and 370 mm). From these figures, it is noticeable that the energy (area under the graph) absorbed by the tubes due to oblique loading is much lower than for direct loading. Since the oblique loading causes two kinds of mechanical loads onto the tube, namely the axial compression and bending, the tubes under oblique loading bend while undergoing some form of progressive crushing. It is also evident that the force–displacement characteristic for different perimeters within the same geometrical profile is rather similar for both axial and oblique loading. This is an indication that the perimeter does not play an important role in the folding mechanism (progressive collapse) of the tubes.

##### 4.2. Energy absorption

In Figs. 10 and 11, the energy absorption is plotted as a function of the deformation length rather than as a function of time because this facilitates the comparison of different structural

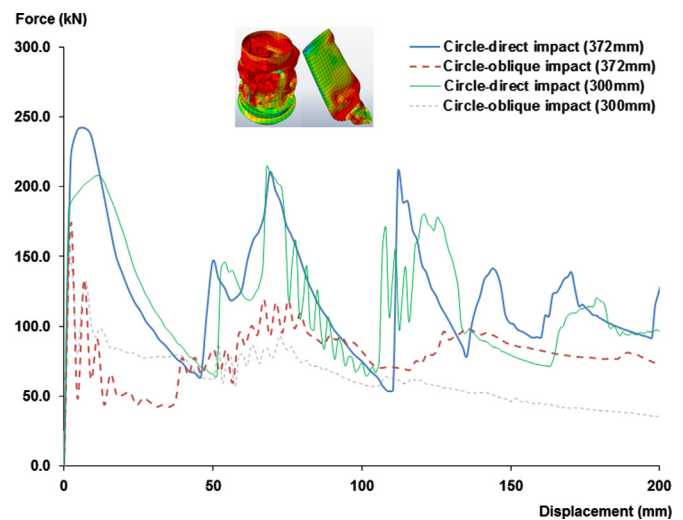


**Fig. 4.** Force vs. displacement for circular tubes (direct and oblique impacts).

design concepts. Based on these figures it can be concluded that the rectangle cross sectional geometry has significantly lower energy absorption than the other five profiles for both impact conditions. These figures also show that the octagonal and hexagonal profiles are better energy absorbers in both loading conditions. A summary of the energy absorption capabilities for all tube profiles is given in Figs. 12 and 13 for both direct and oblique loading respectively. From here, it can be seen that as the perimeter was increased from 300 mm to 372 mm, most profiles exhibited a higher energy absorption capability. In terms of specific energy absorption (SEA), the hexagonal tube with a perimeter profile of 300 mm had the highest SEA compared to the other profiles. This is depicted in Figs. 14 and 15 for direct and oblique loading respectively.

Another view of the energy absorption will be investigating the effects of profiles on the energy absorption due to oblique loading. This is depicted in Tables 7 and 8 for both different perimeters

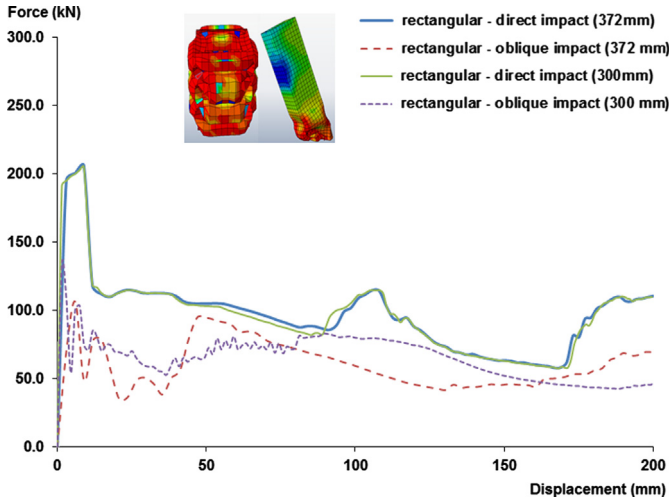


Fig. 5. Force vs. displacement for rectangular tubes (direct and oblique impacts).

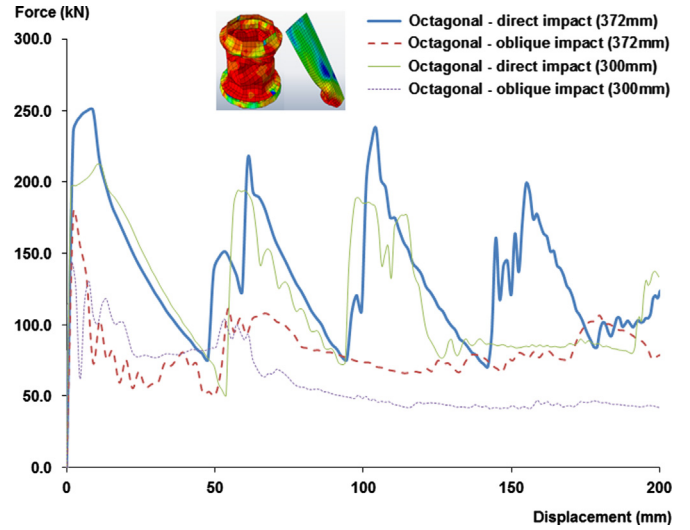


Fig. 8. Force vs. displacement for octagonal tubes (direct and oblique impacts).

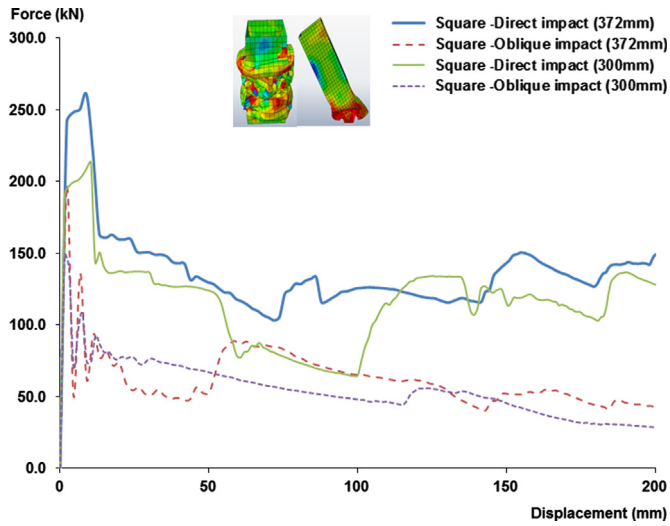


Fig. 6. Force vs. displacement for square tubes (direct and oblique impacts).

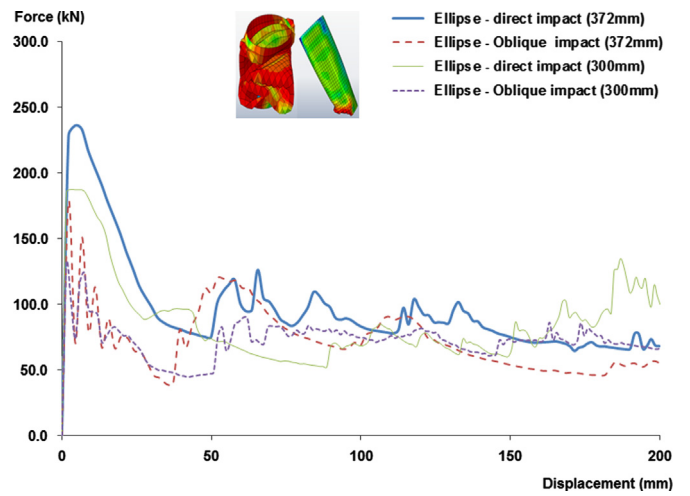


Fig. 9. Force vs. displacement for ellipse tubes (direct and oblique impacts).

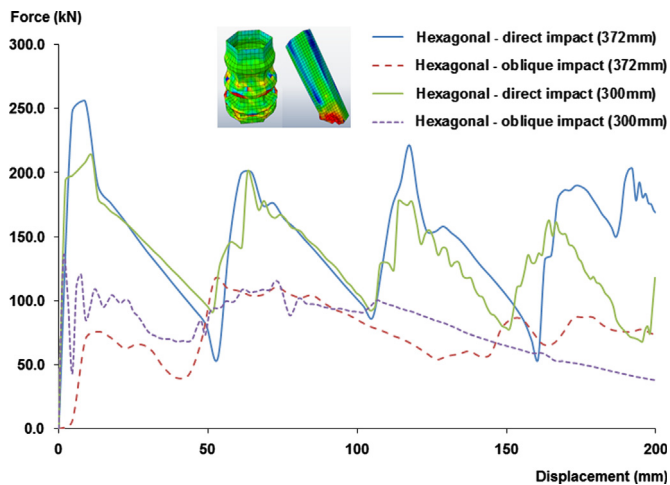


Fig. 7. Force vs. displacement for hexagonal tubes (direct and oblique impacts).

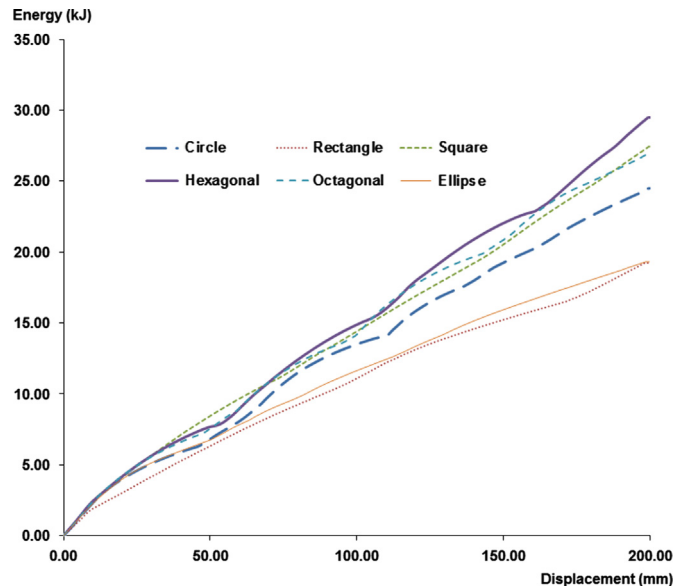


Fig. 10. Energy absorption characteristics of six different profiles for direct impact loading with perimeter 372 mm.

under study. In general it can be concluded that profiles studied with oblique loading showed decreasing energy absorption. The percentage of decrease varied according to the profile time, but on an average the difference is between 15% and 55% for all the

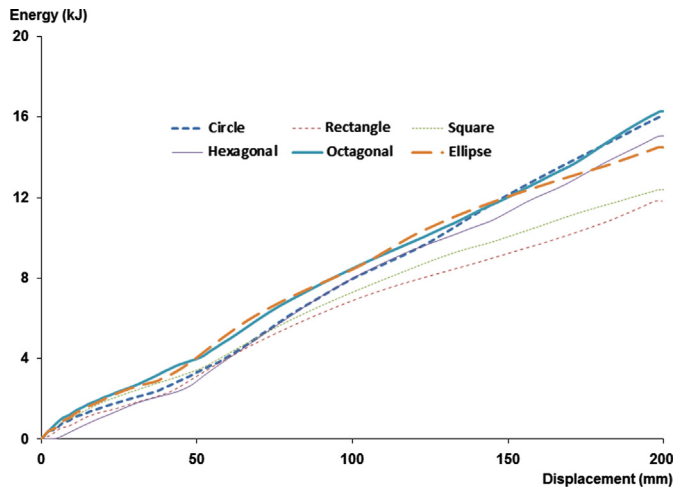


Fig. 11. Energy absorption characteristics of six different profiles for oblique impact loading with perimeter 372 mm.

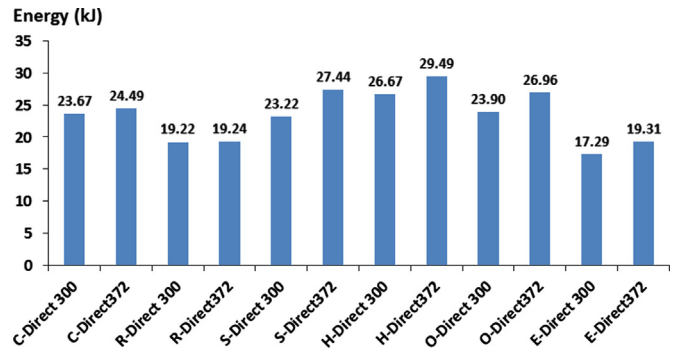


Fig. 12. Energy absorption capability for various profiles due to direct loading condition.

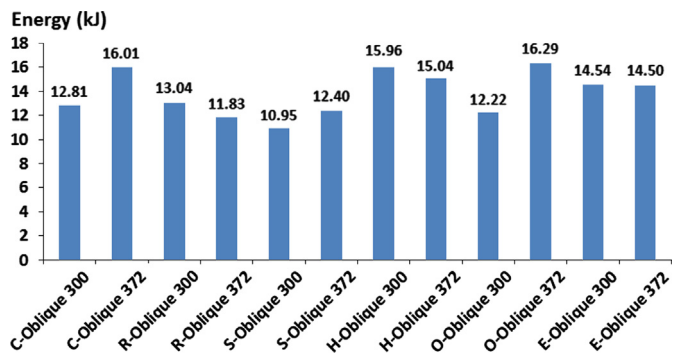


Fig. 13. Energy absorption capability for various profiles due to oblique loading condition.

profiles. Hexagonal, octagonal and circular are good geometry to be considered since they have outstanding performance in terms of energy absorption in both loading and perimeter conditions. The task now is to select the best tube in terms of the geometry profile and also the perimeter. This involves using performance criteria such as energy absorption capabilities, crush force efficiency, cost and manufacturing constraints. This will be discussed in the next section.

4.3. Selection of the best profile

For the multi-criteria decision making (MCDM) process, the complex proportional assessment method (COPRAS) was chosen.

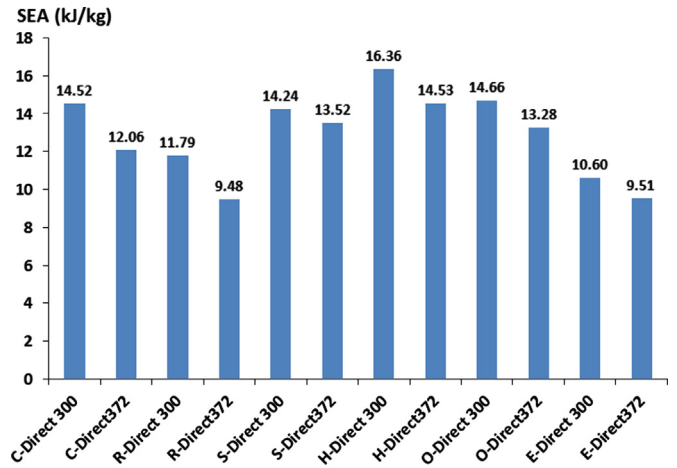


Fig. 14. Specific energy absorption capability for various profiles due to direct loading condition.

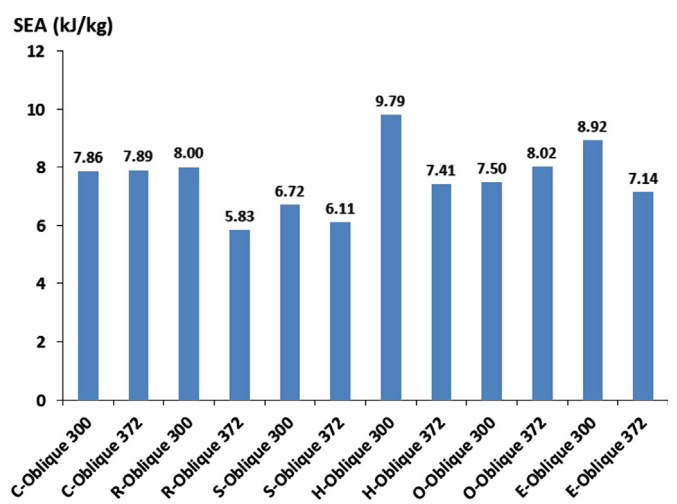


Fig. 15. Specific energy absorption capability for various profiles due to oblique loading condition.

Table 7 Energy absorption of six profiles with two different load conditions.

Shape	Perimeter 372 mm	
	Energy absorption (kJ) Direct Impact 200 mm deformation	Energy absorption (kJ) Oblique Impact 200 mm deformation
Circle	24.49	16.01 -34.63%
Rectangle	19.24	11.83 -38.51%
Square	27.44	12.4 -54.81%
Hexagonal	29.49	15.04 -49.00%
Octagonal	26.96	16.29 -39.58%
Ellipse	19.31	14.5 -24.91%

This method was chosen for its simplicity in usage. The method assumes direct and proportional dependences of the significance and utility degree of the available alternatives under the presence of mutually conflicting criteria. It takes into account the



performance of the alternatives with respect to different criteria and the corresponding criteria weights. This method selects the best decision considering both the ideal and the least preferred solutions. The details of this method have been presented in the previous section.

The first step is to determine the associated weightage for each performance criteria. This is depicted in Table 9. Once the weightages have been assigned to the respective indicators, the decision matrix, as shown in Table 10, is normalized using Eq. (4) and the corresponding weighted normalized decision matrix is developed, as given in Table 11. The purpose of normalization is to obtain dimensionless values of different performance indicators so that all these criteria can be compared. This is followed by computing the sums of the weighted normalized values for both the beneficial attributes and non-beneficial attributes as given in Table 12. In this case the only non-beneficial attribute is the ratio indicator where a lower value is preferred. Then, applying Eq. (11) the relative significance or priority value ( $Q_i$ ) for each tube concept is determined, as shown in Table 13. This table also exhibits the value of quantitative utility ( $U_i$ ) for each tube concept on the basis of which the complete ranking of the tube concept is obtained. The candidate tube for designing an efficient energy absorber is hexagonal with a perimeter of 300 mm, followed by hexagonal with a perimeter of 372 mm. The worst concept is the square profile. Hence, it is the hexagonal tube with a perimeter of 300 mm that was chosen for the next phase of the study which is to investigate the effects of thickness and foam filling in the enhancement of energy absorption.

**Table 8**  
Energy absorption of six profiles with two different load conditions.

Shape	Perimeter 300 mm	
	Energy absorption (kJ) Direct Impact 200 mm deformation	Energy absorption (kJ) Oblique Impact 200 mm deformation
	Circle	23.67
Rectangle	19.22	13.04 -32.15%
Square	23.22	10.95 -52.84%
Hexagonal	26.67	15.96 -40.16%
Octagonal	23.9	12.22 -48.87%
Ellipse	17.29	14.54 -15.91%

**Table 9**  
Weightage setting for each performance indicator.

Performance indicators	Runs, $N = n(n-1)/2$ ( $n$ = number of performance indicators)										$\Sigma$	$\Sigma/E$
	1	2	3	4	5	6	7	8	9	10		
A.E (D) KJ	2	3	3	2							10	0.250
A.E (O) KJ	2				3	3	2				10	0.250
C.F.E(D)		1			1			2	2		6	0.150
C.F.E(O)			1			1		2		2	6	0.150
Ratio				2			2		2	2	8	0.200
		A.E (D) KJ	Energy absorbed (direct loading)							E=	40	1
		A.E (O) KJ	Energy absorbed (oblique loading)									
		C.F.E(D)	Crash force efficiency (direct loading)									
		C.F.E(O)	Crash force efficiency (oblique loading)									
		Ratio	A.E (D)/ A.E (O)									

4.4. Effect of foam and thickness on energy absorption

In this phase of study, the selected tube from phase 1, namely the hexagonal tube with a perimeter of 300 mm was further investigated in terms of tube wall thickness and foam filling. The wall thicknesses selected were 1 mm, 2 mm and 3 mm. The detailed results are presented in Table 14. From this investigation, it was found that for the tubes filled with foam, the effect of

**Table 10**  
Data of performance indicators in a decision matrix.

Specimens	Weightages				
	0.25	0.25	0.15	0.15	0.2
	Performance indicators				
	A.E (D)	A.E (O)	CFE(D)	CFE(O)	Ratio
C_300	23.67	12.81	0.55	0.41	1.85
C_372	24.49	16.01	0.49	0.46	1.53
R_300	19.22	13.04	0.46	0.48	1.47
R_372	19.24	11.83	0.46	0.56	1.63
S_300	23.22	10.95	0.55	0.36	2.12
S_372	27.44	12.40	0.52	0.31	2.21
H_300	26.67	15.96	0.60	0.59	1.67
H_372	29.49	15.04	0.59	0.64	1.96
O_300	23.90	12.22	0.55	0.42	1.96
O_372	26.96	16.29	0.52	0.46	1.66
E_300	17.29	14.54	0.46	0.56	1.19
E_372	19.31	14.50	0.39	0.40	1.33

**Table 11**  
Weighted normalized decision matrix.

Specimens	Weightages				
	0.25	0.25	0.15	0.15	0.2
	Performance indicators				
	A.E (D)	A.E (O)	CFE(D)	CFE(O)	Ratio
C_300	0.021	0.019	0.013	0.011	0.018
C_372	0.022	0.024	0.012	0.012	0.015
R_300	0.017	0.020	0.011	0.013	0.014
R_372	0.017	0.018	0.011	0.015	0.016
S_300	0.021	0.017	0.014	0.010	0.021
S_372	0.024	0.019	0.013	0.008	0.022
H_300	0.024	0.024	0.015	0.016	0.016
H_372	0.026	0.023	0.014	0.017	0.019
O_300	0.021	0.018	0.014	0.011	0.019
O_372	0.024	0.025	0.013	0.012	0.016
E_300	0.015	0.022	0.011	0.015	0.012
E_372	0.017	0.022	0.010	0.011	0.013

thickness after 2 mm is not significant for both direct and impact loading. This is because of the increases in the apparent stiffness of the structure due to the foam filling. The same goes for the crush force efficiency. In general, foam filling does improve the crash performance indicators. The pictorial representation is depicted in Figs. 16 and 17.

4.5. Effect of trigger mechanism

Notch-based trigger mechanism was used to reduce the peak force and to encourage progressive crushing. From the second phase, the 2 mm wall thickness hexagonal tube with foam filling was chosen. A circular notch of radius 10 mm was introduced 10 mm below the top opening of the tube. The results showed that the peak force was reduced from 316 kN to 284 kN without compromising the energy absorption capability. The CFE increased from 0.75 to 0.80 (7% increase). The overall crushing mechanism was more progressive as shown in Fig. 18.

Table 12  
Sums of the weighted normalized values.

Specimens	Beneficial Si+	Non Beneficial Si-
C_300	0.065	0.018
C_372	0.07	0.015
R_300	0.061	0.014
R_372	0.061	0.016
S_300	0.06	0.021
S_372	0.064	0.022
H_300	0.078	0.016
H_372	0.08	0.019
O_300	0.064	0.019
O_372	0.073	0.016
E_300	0.063	0.012
E_372	0.059	0.013
Σ	0.8	0.2

Table 13  
Qi and Ui values.

Specimens	Q	U	Rank
CIR_300	0.080	84.119	7
CIR_372	0.088	93.313	4
Rec_300	0.080	84.037	8
Rec_372	0.078	82.369	10
Sq_300	0.073	77.555	12
Sq_372	0.077	80.908	11
Hex_300	0.095	100.000	1
Hex_372	0.094	99.786	2
Oct_300	0.079	82.944	9
Oct_372	0.090	95.219	3
ELL_300	0.087	91.517	5
ELL_372	0.080	84.645	6

Table 14  
Comparison of thickness, foam filling and impact angle for the hexagonal tube of length 300 mm.

Indicators	Direct no foam			Direct with foam			Oblique no foam			Oblique with foam		
	1 mm	2 mm	3 mm	1 mm	2 mm	3 mm	1 mm	2 mm	3 mm	1 mm	2 mm	3 mm
Energy (kJ)	16.87	26.82	30.61	28.79	30.71	30.68	5.35	16.12	28.66	17.62	29.78	30.73
Pmax (kN)	185.80	211.64	343.00	245.96	316.34	406.83	47.38	112.05	185.71	80.66	158.24	261.15
CFE	0.32	0.63	0.74	0.61	0.75	0.79	0.56	0.71	0.77	0.74	0.75	0.75
Faverage (kN)	58.93	134.00	255.26	150.31	235.93	320.89	26.63	80.07	143.19	65.33	117.92	196.00

5. Conclusion

A numerical investigation of the axial and oblique crush responses of thin walled, ductile metallic alloy (mild steel A36) of various cross sectional profiles was performed. The investigation was broken up into three phases: (1) the investigation of individual cross sectional profile and the selection of the best profile, (2) the investigation of tube wall thickness and foam filling on the crush response on the chosen profile and finally (3) the effect of trigger mechanism onto the selected profile design.

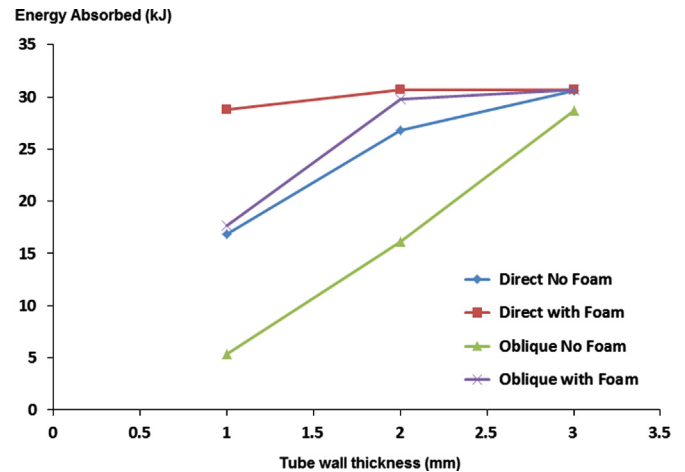


Fig. 16. Effect of tube wall thickness and foam on the energy absorption capability for the hexagonal tube.

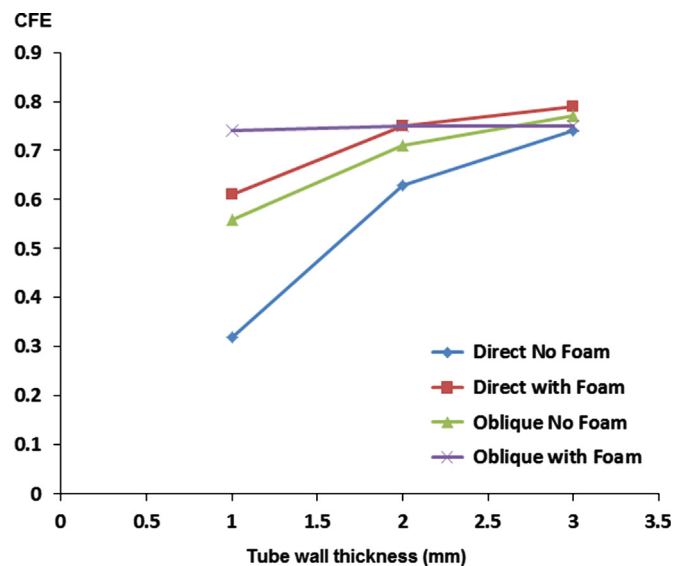


Fig. 17. Effect of tube wall thickness and foam on the crush force efficiency (CFE) for the hexagonal tube.

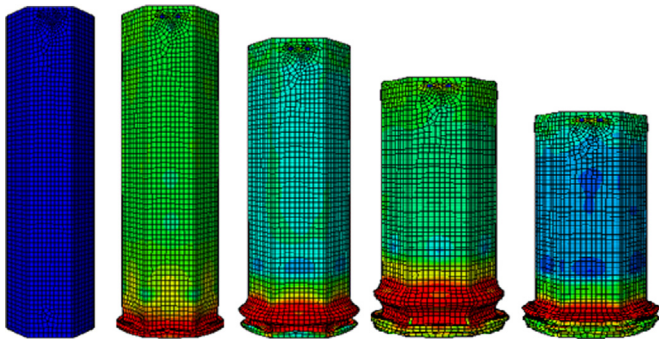


Fig. 18. Progressive crushing of hexagonal tube due to trigger mechanism.

All simulations were dynamic with an impact speed of 15 m/s and impact mass of 275 kg. Oblique loading was simulated at a 30° angle to the tube's axial direction. It was found that the hexagonal profile was a better concept for energy absorption application taking into account the crash performance indicators as well as the cost and manufacturing feasibility. The 2 mm thickness hexagonal tube had an energy absorption of 26 kJ and a CFE of 0.68 for direct loading and an energy absorption of 16 kJ and a CFE of 0.71 for oblique loading. When foam filling was added, the crash performance indicators improved. For direct and oblique loading, the 2 mm thickness hexagonal tube had an energy absorption of 30 kJ and a CFE of 0.75 respectively. This is a remarkable improvement for the oblique impact crush performance. Finally, the trigger mechanism in the form of a hole induced in the tube helped to lower the peak force and improve the crash force efficiency to 0.80. This is partly due to the more effective progressive crushing that was introduced by the trigger mechanism. In conclusion, it can be stated that the hexagonal tube of wall thickness 2 mm with aluminum foam filling and a trigger mechanism has shown to be of good potential as an energy absorber candidate for crashworthiness application to help mitigate serious injuries to the occupant of the vehicle.

## Acknowledgment

The authors would like to thank the Malaysian Ministry of Science, Technology and Innovation (MOSTI) for the support of this research program (03-02-03SF0216).

## References

- [1] Guoxing L, Tongxi Y. Energy absorption of structures and materials. England: Woodhead Publishing Limited; 1–23.
- [2] Jones N. Structural impact. Cambridge, UK: Cambridge University Press; 1989.
- [3] Qi Chang, Yang Shu, Dong Fangliang. Crushing analysis and multiobjective crashworthiness optimization of tapered square tubes under oblique impact loading. *Thin-Walled Structures* 2012;59:103–19.
- [4] Zhou Yunjiao, Lan Fengchong, Chen Jiqing. Crashworthiness research on S-shaped front rails made of steel aluminum hybrid materials. *Thin-walled Structures* 2011;49:291–7.
- [5] Ramakrishna S, Hamada H. Energy absorption characteristics of crashworthy structural composite materials. *Key Engineering Materials* 1998;141–143:585–620.
- [6] Olabi AG, Morris Edmund, Hashmi MSJ. Metallic tube type energy absorbers: a synopsis. *Thin Walled Structures* 2007;45:707–26.
- [7] Nagel Gregory. Impact and energy absorption of straight and tapered rectangular tubes. Australia: Queensland University of Technology; 2005 PhD thesis.
- [8] Borvik T, Hopperstad OS, Reyes A, Langseth M, Solomos G, Dyngeland T. Empty and foam filled circular aluminum tubes subjected to axial and oblique quasi static loading. *International Journal of Crashworthiness* 2003;8:481–94.
- [9] Reyes A, Langseth M, Hopperstad OS. Crashworthiness of aluminum subjected to oblique loading: experiments and numerical analyses. *International Journal of Mechanical Sciences* 2002;44:1965–84.
- [10] Reyes A, Langseth M, Hopperstad OS. Aluminum foam filled extrusions subjected to oblique loading: experiments and numerical analyses. *International Journal of Solids and Structures* 2002;44:1645–75.
- [11] Reyes A, Langseth M, Hopperstad OS. Square aluminum tubes subjected to oblique loading. *International Journal of Impact Engineering* 2003;28(10):1077–106.
- [12] Reid SR, Reddy TY. Static and dynamic crushing of tapered sheet metal tubes of rectangular cross section. *International Journal of Mechanical Sciences* 1986;28:623–37.
- [13] Cho Yong-Bum, Bae Chul-Ho, Suh Myung-Won, Sin Hyo-Chol. A vehicle front frame crash design optimization using hole-type and dent-type crush initiator. *Thin Walled Structures* 2006;44:415–28.
- [14] Reddy TY, Wall RJ. Axial compression of foam filled thin walled circular tubes. *International Journal of Impact Engineering* 1988;7(2):151–66.
- [15] Sherwood JA, Frost CC. Constitutive modeling and simulation of energy absorbing polyurethane foam under impact loading. *Polymer Engineering and Science* 1992;32(16):1138–46.
- [16] Seitzberger M, Rammerstorfer FG, Gradinger R, Degischer HP, Blaimachein M, Walch C. Experimental studies on the quasi static axial crushing of steel columns filled with aluminum foam. *International Journal of Solids and Structures* 2000;37(30):4125–47.
- [17] Toksoy AK, Guden M. The strengthening effect of polystyrene foam filling in aluminum thin walled cylindrical tubes. *Thin-Walled Structures* 2005;43(2):333–50.
- [18] Tarlochan F, Ramesh S, Harpreet S. Advanced composite sandwich structure design for energy absorption applications: blast protection and crashworthiness. *Composites Part B: Engineering* 2012;43(5):2198–208.
- [19] Tarlochan F, Ramesh S. Composite sandwich structure with nested inserts for energy absorption application. *Composite Structures* 2012;94(3):904–16.
- [20] Tarlochan F, Hamouda AMS, Sahari BB, Mahdi E. Composite sandwich structures for crashworthiness applications. *Proceedings of the Institution of Mechanical Engineers, Part L: Journal Of Material: Design and Application* 2007;221(2):121–30.
- [21] Lanzi L, Castelletti LML, Anghileri M. Multi-objective optimization of composite absorber shape under crashworthiness requirements. *Composite Structures* 2004;65:433–41.
- [22] Fyllingen O, Hopperstad OS, Hanssen AG, Langseth M. Modelling of tubes subjected to axial crushing. *Thin Walled Structures* 2010;48:134–42.
- [23] Chatterjee Prasenjit, Manikrao Athawale Vijay, Chakraborty Shankar. Materials selection using complex proportional assessment and evaluation of mixed data methods. *Materials and Design* 2011;32:851–60.
- [24] Dehghan-Manshadi B, Mahmudi H, Abedian A, Mahmudi R. A novel method for materials selection in mechanical design: Combination of non-linear normalization and a modified digital logic method. *Materials and Design* 2007;28:8–15.
- [25] Witteman WJ. Improved vehicle crashworthiness design by control of the energy absorption for different collisions situation. Netherlands: Eindhoven University of Technology; 1999 PhD thesis.
- [26] Olabi AG, Morris E, Hashmi MSJ, Gilchrist MD. Optimised design of nested circular tube energy absorbers under lateral impact loading. *International Journal of Mechanical Sciences* 2008;50:104–16.
- [27] Ahmad Z, Thambiratnam DP. Dynamic computer simulation and energy absorption of foam-filled conical tubes under axial impact loading. *Computers and Structures* 2009;87:186–97.
- [28] Duan CZ, Dou T, Cai YJ, Li YY. Finite element simulation and experiment of chip formation process during high speed machining of AISI 1045 hardened steel. *International Journal of Recent Trends in Engineering* 2009;1(5):46–50.
- [29] Dean J, Dunleavy CS, Brown PM, Clyne TW. Energy absorption during projectile perforation of thin steel plates and the kinetic energy of ejected fragments. *International Journal of Impact Engineering* 2009;36(10–11):1250–8.
- [30] Lacy JM, Shelley JK, Weathersby JH, Daehn GS, Johnson J, Taber G. Optimization-based constitutive parameter identification from Sparse Taylor cylinder data. In: *Proceedings of the 81st shock and vibration symposium*. Idaho National Laboratory, US; 2010.
- [31] Deshpande VS, Fleck NA. Isotropic constitutive models for metallic foams. *Journal of the Mechanics and Physics of Solids* 2000;48:1253–83.
- [32] Shabbeyk S, Spettrinic N, Vafai A. Numerical modelling of dynamically loaded metal foam-filled square columns. *International Journal of Impact Engineering* 2007;34:573–86.
- [33] Ahmad Z, Thambiratnam DP. Dynamic computer simulation and energy absorption of foam-filled conical tubes under axial impact loading. *Computers and Structures* 2009;87(3–4):186–97.
- [34] Reyes A, Hopperstad OS, Berstad T, Hanssen AG, Langseth M. Constitutive modeling of aluminum foam including fracture and statistical variation of density. *European Journal of Mechanics A: Solids* 2003;22(6):815–35.